



Journal Name

ARTICLE TYPE

Central substitution of azacalixphyrins: a strategy to acidochromic NIR dyes: ESI

Cite this: DOI: 10.1039/xxxxxxxxxx

Cloé Azarias,^a Simon Pascal,^b Olivier Siri,^{*b} and Denis Jacquemin^{*a}

Received Date
Accepted Date

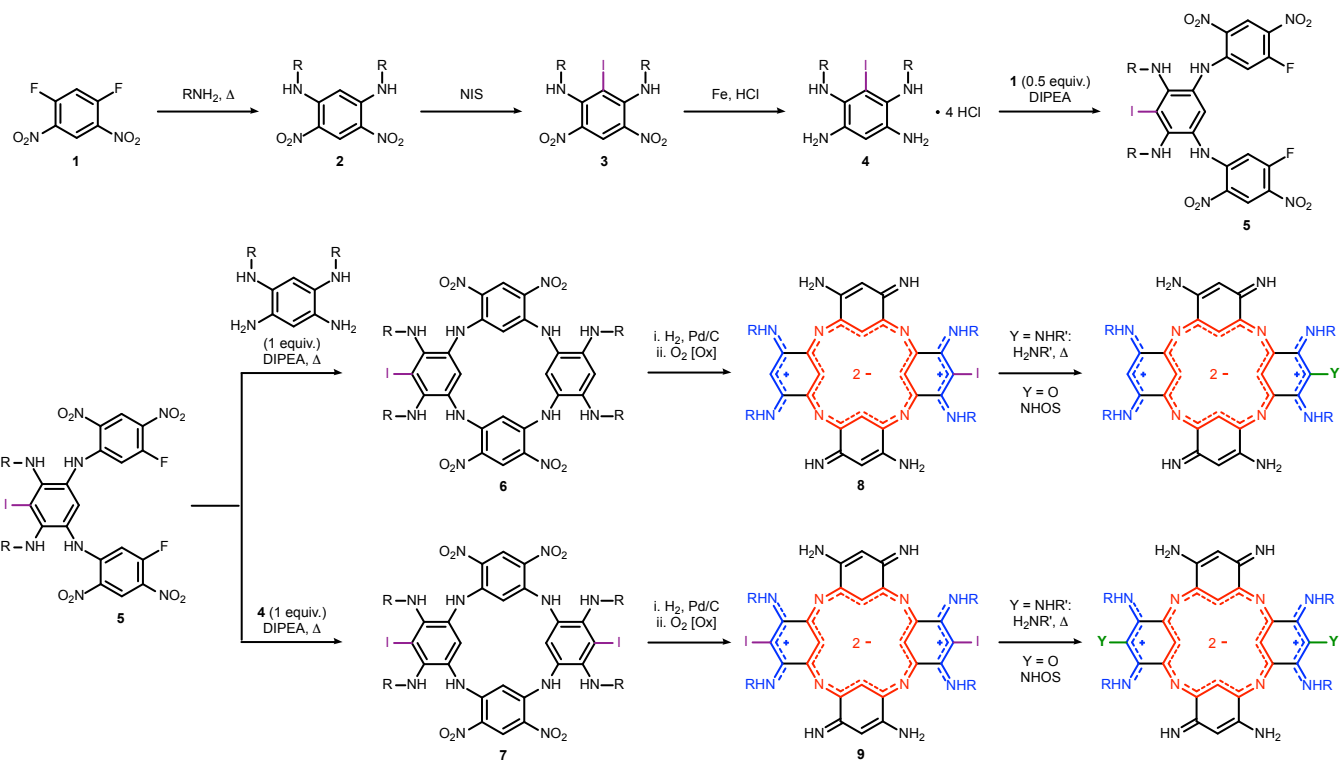
DOI: 10.1039/xxxxxxxxxx

www.rsc.org/journalname

^a Chimie Et Interdisciplinarité, Synthèse, Analyse, Modélisation (CEISAM), UMR CNRS no. 6230, BP 92208, Université de Nantes, 2, Rue de la Houssinière, 44322 Nantes, France. E-mail: Denis.Jacquemin@univ-nantes.fr

^b Aix Marseille Univ, CNRS-CINAM, Campus de Luminy, Case 913, 13288 Marseille Cedex 09, France. E-mail: olivier.siri@univ-amu.fr

S1 Possible synthetic route to Y-substituted ACPs



Scheme S1.1 Enisaged synthetic route to Y-substituted ACP. NIS stands for N-iodosuccinimide, DIPEA is diisopropylethylamine, and NHOS is N-hydroxysuccinimide.

S2 Characterisation of the ACP parent

The representation of the protonation states of the unsubstituted ACP discussed below are given in Figure S1

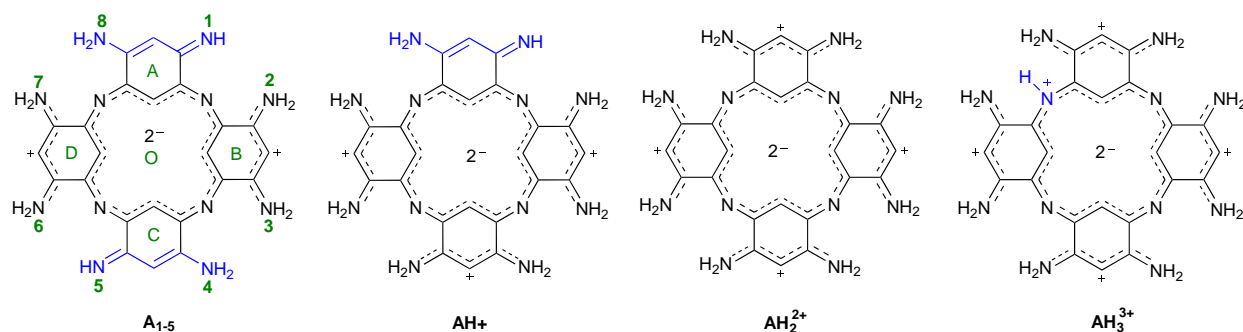


Fig. S1 Representation of the structures of the different protonation states of the ACP molecule. The changes upon protonation/deprotonation of the parent di-protonated AH_2^{2+} are highlighted in blue. For the non-protonated compound **A** (left), one tautomer in which the imine groups are at positions **1** and **5** is represented and it is therefore named **A**₁₋₅. The numbering of these positions is represented in green in this structure together with the labels for the NICS centres (O, A, B, C, and D).

S2.1 Geometry, stability, and aromaticity

The geometry of the parent azacalixphyrin has been described both theoretically and experimentally,¹ and consistently with these previous investigations, saddle-like non planar structures were obtained, a conclusion holding irrespective of the protonation state of the macrocycle (see Figure S2).

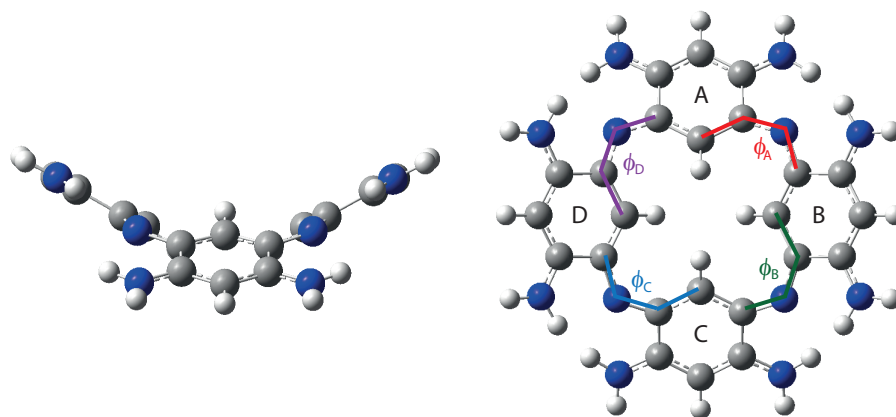


Fig. S2 Side (left) and top (right) views of the optimised structure of AH_2^{2+} . The labels of the phenyl-like rings (A, B, C, and D) and key dihedral angles (ϕ_A , ϕ_B , ϕ_C , and ϕ_D) are displayed on the ACP structure on the left.

To evaluate the sensitivity of the macrocycle to protonation/deprotonation, we examined the distortion from planarity through the analysis of the dihedral angles ϕ between the internal CC bond of a given phenyl ring and the bridge as illustrated in Figure S2. The values of these angles are listed in Table S1. Consistently with Ref. 2, the di-protonated macrocycle present a dihedral distortion of 22° , the expected value for a completely planar macrocycle being of course $\phi = 0^\circ$. The protonation of AH_2^{2+} further distorts the macrocycle from planarity, with in particular the dihedral angle ϕ_D that reaches 26° , an expected change since this angle comprises the protonated nitrogen atom. Upon deprotonation, more intricate effects are observed. For AH^+ , the dihedral angle ϕ_A (A being the ring with the deprotonated amine group at position 1) and ϕ_C are almost unchanged (23°) compared to AH_2^{2+} , whereas ϕ_B and ϕ_D respectively present a smaller (20°) and larger (26°) distortion from planarity than their di-protonated counterpart. For doubly protonated species, i.e., when going from AH_2^{2+} to neutral **A** forms, the dihedral angles range from 18 to 29° . The smallest differences between the four dihedral angles within a given central cycle are observed for the most symmetric **A**₁₋₅ tautomer (with ϕ angles of 22 – 24°) whereas the largest differences (reaching 10°) are obtained for **A**₁₋₂ and **A**₁₋₃ forms that both present two imine function on two vicinal six-membered rings, namely A and B.

The relative stabilities of the tautomers of the non-protonated ACP species are reported in Table S1. Consistently with the theoretical results of Ref. 2, all tautomers, but the very unfavourable **A**₁₋₈ form, present comparable energies and one cannot discriminate the other forms as their energy difference are within the error bar of the used theory for the energies of large solvated species (ca. 1–3 kcal/mol).

Table S1 Relative free energies (ΔG_{LBS} in kcal/mol) of the tautomers of the non-protonated azacalixpyrin. The LBS label refers to the large atomic basis set, 6-311+G(2d,p), and G_{LBS} corresponds to the free energy corrected for basis set effects, i.e., the energetic difference between E_{LBS} and E_{SBS} is added to the value of G_{SBS} . For all the protonated/deprotonated forms of the ACP, the dihedral angles (ϕ_X in degrees, X=A, B, C, or D, see Figure S2) and NICS(0) values at the centre of all rings (in ppm) are given. The numbering of the rings is given in Figure S1. The values in bold corresponds to a phenyl ring bearing one (two in the case of **A₁₋₈**) imine function(s). Note that **A₁₋₇** is not reported as it is equivalent to **A₁₋₃**.

	Energy ΔG_{LBS}	Geometry					Aromaticity (NICS)				
		PG	ϕ_A	ϕ_B	ϕ_C	ϕ_D	O	A	B	C	D
A₁₋₂	0.9	C_2	23	18	23	28	-4.5	6.6	6.6	1.0	1.0
A₁₋₃	0.0	C_1	19	21	29	27	-4.7	6.2	6.9	2.4	0.1
A₁₋₄	1.6	C_s	24	19	19	28	-6.2	6.6	4.4	6.6	0.1
A₁₋₅	2.6	C_2	22	24	22	24	-7.2	7.1	2.6	7.1	2.6
A₁₋₆	1.9	C_2	20	22	25	24	-5.6	6.9	1.8	1.8	6.9
A₁₋₈	13.8	C_s	21	21	23	24	-1.9	11.0	1.5	1.2	1.5
AH⁺	—	C_1	23	20	23	26	-6.7	7.5	5.1	2.8	3.7
AH₂²⁺	—	D_{2d}	22	22	22	22	-8.4	5.7	5.7	5.7	5.7
AH₃³⁺	—	C_2	23	24	26	26	-8.4	3.5	6.2	6.2	3.5

Disregarding the improbable **A₁₋₈** tautomer, one sees that all the azacalixpyrins, irrespective of their protonation state, are strongly aromatic, the NICS(0) values (reported in Table S1) being ordered as: **A** \approx **AH⁺** $>$ **AH₂²⁺** $=$ **AH₃³⁺**, that is, the di- and tri-protonated species present the strongest aromatic character. If it appears intuitive that the highly symmetric **AH₂²⁺** stands as the most aromatic structure, a similar NICS value being interestingly obtained for **AH₃³⁺**. This can be explained as the addition of a hydrogen atom on a bridging nitrogen takes place in the perpendicular plane of the macrocyclic core and therefore does not impact significantly the p electrons of the protonated nitrogen atom that are taking part in the π -conjugation of the central cycle. However, according to the analysis of the dihedral angles, the protonation induces a further distortion from the plane of the phenyl-like rings. Nevertheless, in this case, this distortion is counterbalanced by a homogenisation of the bond length distribution around the protonated nitrogen atom (with vicinal CC and CN bond lengths to the protonated nitrogen atom of 1.377 and 1.371 Å, respectively). Moreover, in contrast to **AH⁺**, **AH₃³⁺** exhibit a symmetric structure (C_2). In the neutral tautomers, the NICS(0) value at the centre of the macrocycles ranges from -5 to -7 ppm, following **A₁₋₂** \approx **A₁₋₃** $>$ **A₁₋₆** $>$ **A₁₋₄** $>$ **A₁₋₅**, consistently with Ref. 2. Interestingly, the most symmetric **A₁₋₅** tautomer (in terms of both point group symmetry and spatial arrangement), that is also the less distorted form from the di-protonated structure, is the one displaying the strongest aromatic character. Note that for **A₁₋₈**, while the NICS value at the centre of the macrocycle remains negative (-2 ppm) it is largely increased compared to the other tautomers which indicates that this macrocycle is poorly aromatic compared to the others, which is perfectly consistent with the large instability of **A₁₋₈** revealed by the free energies analysis. Regarding the NICS(0) values obtained for the constitutive phenyl-like rings (A, B, C, and D), all the centres present a positive NICS value demonstrating their anti-aromatic [or non aromatic for NICS(0) values close to 0 ppm] character. The anti-aromaticity of the ring A in **A₁₋₈** bearing two imine (NH) functions is more pronounced [NICS(0)=11 ppm] than in the rings bearing one imine group [NICS(0) of ca. 6–7 ppm] that is itself larger than in the rings bearing two amino (NH₂) functions [NICS(0)=0.1–4.4 ppm], which is a logical consequence of their Lewis structure (see Figure S3). This trend can also be related to the (single) CC bond lengths between the central cycle and the peripheral subunits: the longer are the CC bonds, the more pronounced is the anti-aromatic character of the ring. This outcome also holds when turning to CC bond lengths of the phenyl-like rings in **AH₃³⁺**. Indeed, the two phenyl rings close to the protonated bridging nitrogen (A and D cycles with CC bond lengths of 1.46–1.47 Å) are less anti-aromatic than the two others (B and C rings with CC bond lengths of 1.48 Å).

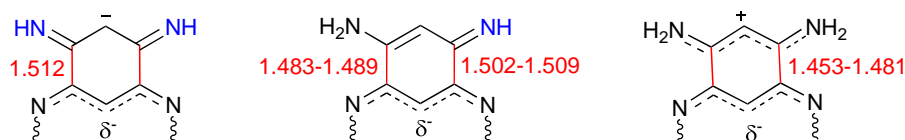


Fig. S3 Structures of the possible phenyl-like moieties present in neutral ACP tautomeric forms. The imine functions are highlighted in blue whereas the single CC bond and their bond length (in Å) are displayed in red.

S2.2 Optical properties

Let us now discuss the optical properties of the ACP monomer. In Figure S4, a comparison between the experimental and theoretical spectra is given. For the non-protonated compound, several tautomers have been identified to co-exist in solution, i.e., A_{1-2} , A_{1-3} , A_{1-4} , A_{1-5} , and A_{1-6} (*vide supra*). The long-wavelength bands of the different tautomers do not appear at the same energies probably explaining why this band is broad in the experimental spectrum of the non-protonated form.¹ For all the protonated species, for which no tautomeric equilibria exist making comparisons more straightforward, theory provides systematically blueshifted absorption bands (by 0.1–0.2 eV) compared to experiments, the gap between the first and second peaks being well-reproduced by TD-DFT with a maximal error of 0.10 eV compared to experiment. At this stage, these blueshifts can be attributed to the lack of vibronic couplings in our calculations.

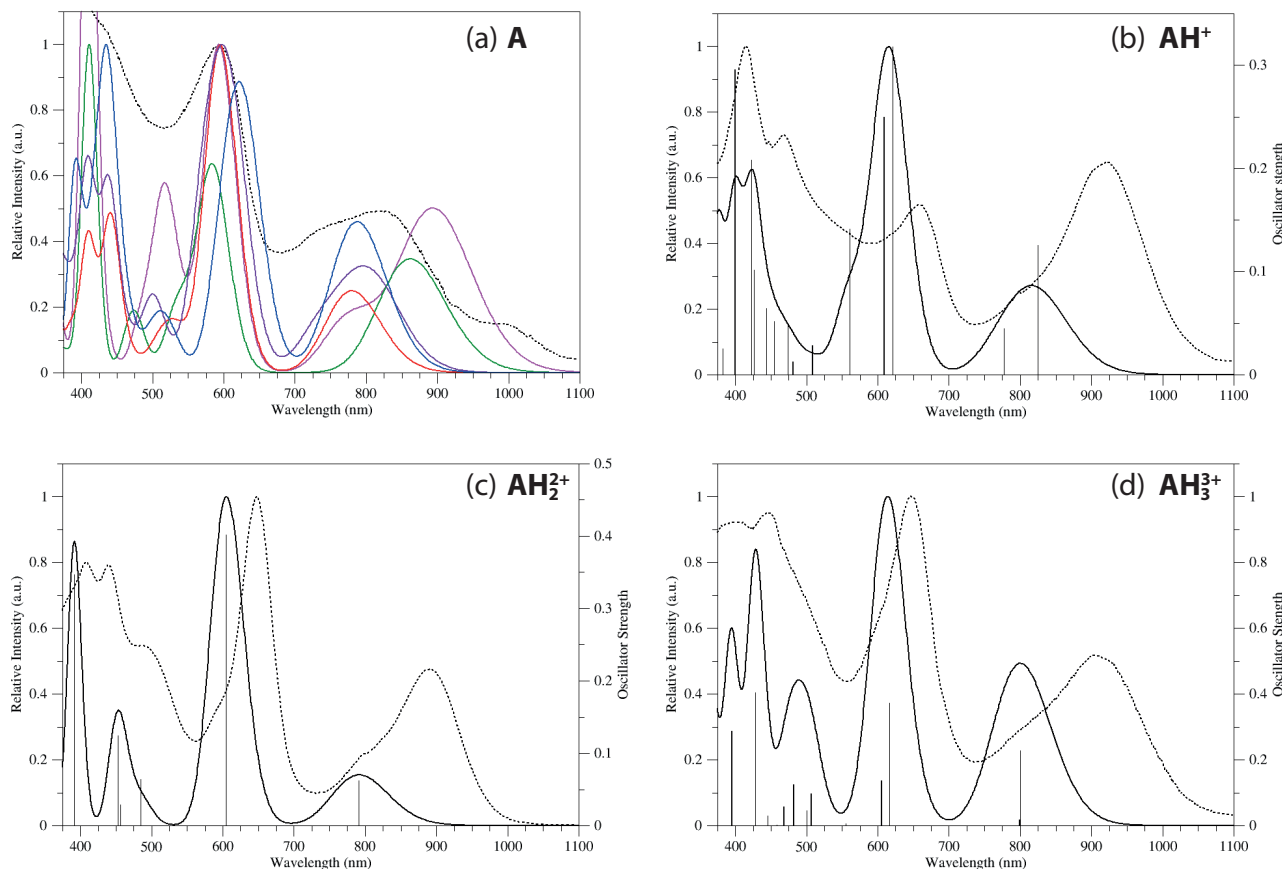


Fig. S4 Normalised experimental (dotted line)³ and theoretical [PCM-PBE0/6-311+G(2d,p)] absorption spectra (full line) of (a) **A**; (b) **AH⁺**; (c) **AH₂²⁺**; and (d) **AH₃³⁺**. The sticks have been convoluted with a Gaussian function with a full width at half-maximum (FWHM) of 1500 cm⁻¹. For the non-protonated molecule, the spectra of all the co-existing tautomers, i.e., A_{1-2} (red) A_{1-3} (violet), A_{1-4} (green), A_{1-5} (magenta), and A_{1-6} (blue) are reported and the stick have been omitted for the sake of clarity. The transition energies, oscillator strengths, and molecular orbital composition of the first four electronic transitions responsible for the two main absorption bands in the visible-NIR region of the spectrum are given in Table S2 whereas the molecular orbitals involved in these transitions are displayed in Figure S5.

When going from the di-protonated form to its mono- or tri-protonated counterparts, theory nicely reproduces the experimental trend, that is, a redshift of the long-wavelength band. However, while one observes a redshift of that band when going from AH^+ to the fully-protonated AH_3^{3+} species, the reverse trend is predicted by theory. Let us underline that we deal here with a very small difference, the longest-wavelength in AH^+ and AH_3^{3+} differing by 0.03 eV only, which is much below the expected accuracy of TD-DFT for such organic molecules.⁴ Moreover, one notices that theory underestimates (overestimates) the intensity of the band at ca. 900 nm for the mono- and the di-protonated (tri-protonated) ACPs compared to the measurements, but with errors again within the expected margin for TD-DFT. From these findings, it appears necessary to assess the accuracy of the TD-PBE0 level of theory for the description of the optical properties of azacalixphyrins, which is done in the main text.

Table S2 PCM-PBE0/6-311+G(2d,p) vertical absorption wavelengths (λ_{abs} in nm), oscillator strengths (f), and contributions of the molecular orbitals involved in the first four electronic transitions of the protonated and non-protonated azacalixpyrins. The molecular orbitals are displayed in Figure S5. The results for \mathbf{A}_{1-8} are not reported as this tautomer is very unstable ($\Delta G > 15$ kcal/mol). H and L stand for HOMO and LUMO, respectively.

Monomer	ES n°	λ_{abs}	f	Molecular orbitals composition
\mathbf{A}_{1-2}	1	780	0.16	H→L (78%), H-1→L+1 (21%)
	2	658	0.00	H-1→L (81%), H→L+1 (18%)
	3	596	0.25	H-1→L+1 (74%), H→L (20%)
	4	594	0.39	H→L+1 (72%), H-1→L (19%)
\mathbf{A}_{1-3}	1	805	0.13	H→L (81%), H-1→L+1 (13%)
	2	739	0.07	H→L+1 (48%), H-1→L (45%)
	3	610	0.35	H-1→L (48%), H→L+1 (47%)
	4	575	0.27	H-1→L+1 (76%), H→L (14%)
\mathbf{A}_{1-4}	1	862	0.25	H→L (93%)
	2	802	0.00	H-1→L (84%), H→L+1 (15%)
	3	585	0.44	H→L+1 (75%), H-1→L (14%)
	4	572	0.01	H-2→L (82%), H-1→L+1 (16%)
\mathbf{A}_{1-5}	1	895	0.21	H→L (90%)
	2	779	0.07	H-1→L (76%), H→L+1 (19%)
	3	614	0.00	H-2→L (99%)
	4	593	0.41	H→L+1 (76%), H-1→L (19%)
\mathbf{A}_{1-6}	1	789	0.19	H→L (76%), H-1→L+1 (22%)
	2	773	0.03	H-1→L (51%), H→L+1 (48%)
	3	629	0.31	H→L+1 (51%), H-1→L (47%)
	4	603	0.17	H-1→L+1 (73%), H→L (20%)
\mathbf{AH}^+	1	825	0.13	H→L (79%), H-1→L+1 (19%),
	2	777	0.04	H-1→L (57%), H→L+1 (39%)
	3	621	0.32	H→L+1 (41%), H-1→L (30%), H-1→L+1 (17%)
	4	609	0.25	H-1→L+1 (49%), H-2→L (16%), H→L+1 (16%)
\mathbf{AH}_2^{2+}	1/2	791	0.12	H-1→L (26%), H-1→L+1 (26%), H→L+1 (24%), H→L (24%)
	3/4	605	0.80	H→L (25%), H→L+1 (25%), H-1→L (23%), H-1→L+1 (23%)
\mathbf{AH}_3^{3+}	1	800	0.23	H→L (78%), H-1→L+1 (20%)
	2	799	0.02	H-1→L (62%), H→L+1 (37%)
	3	617	0.37	H→L+1 (59%), H-1→L (36%)
	4	605	0.14	H-1→L+1 (75%), H→L (18%)

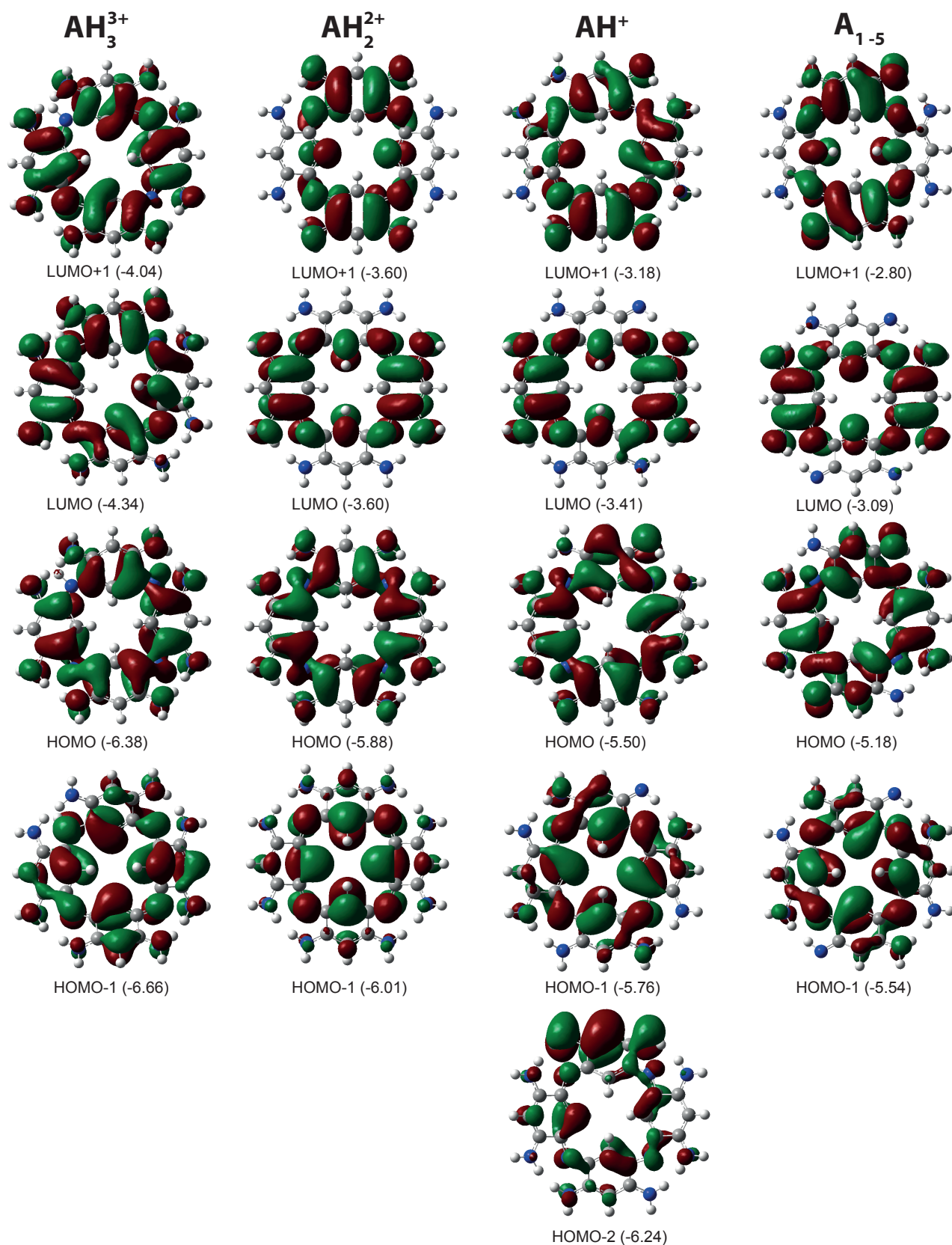


Fig. S5 Topology (isovalue=0.02 a.u.) and energies (given in eV in parenthesis) of the molecular orbitals involved in the first four electronic transitions (reported in Table S2) of the non-protonated and protonated ACP monomers obtained at the PCM-PBE0/6-311+G(2d,p) level of theory. For the non-protonated compound, only the MOs of the most symmetric A_{1-5} tautomer are displayed.

To further characterise the excitations, the electronic density reorganisation upon absorption for the protonated and non protonated (A_{1-5}) species have been calculated at the TD-PBE0 level and the corresponding plots are displayed in Figure S6. First, one sees that all states present a strong density reorganisation indicating highly delocalised phenomena, consistently with NIR absorption. Regarding both the tri- and di-protonated species that possesses eight (zero) peripheral amine (imine) functions, no significant charge-transfer (CT) is observed. In contrast, a partial charge-transfer from the external $NH_2-C=C-C=NH$ subsystems to the cyanine-like ones occurs in the mono-protonated form. Consistently with previous work in the group,¹ the neutral form A_{1-5} form shows transitions involving partial CT (S_1) and more symmetric (S_4) character. These outcomes suggest that the absorption of ACPs behave differently upon solvent modification depending on its protonation state. For instance, while no significant changes of the absorption spectrum of AH_2^{2+} should be observed when going from an apolar to a polar medium, AH^+ is predicted to be a solvatochromic dye.

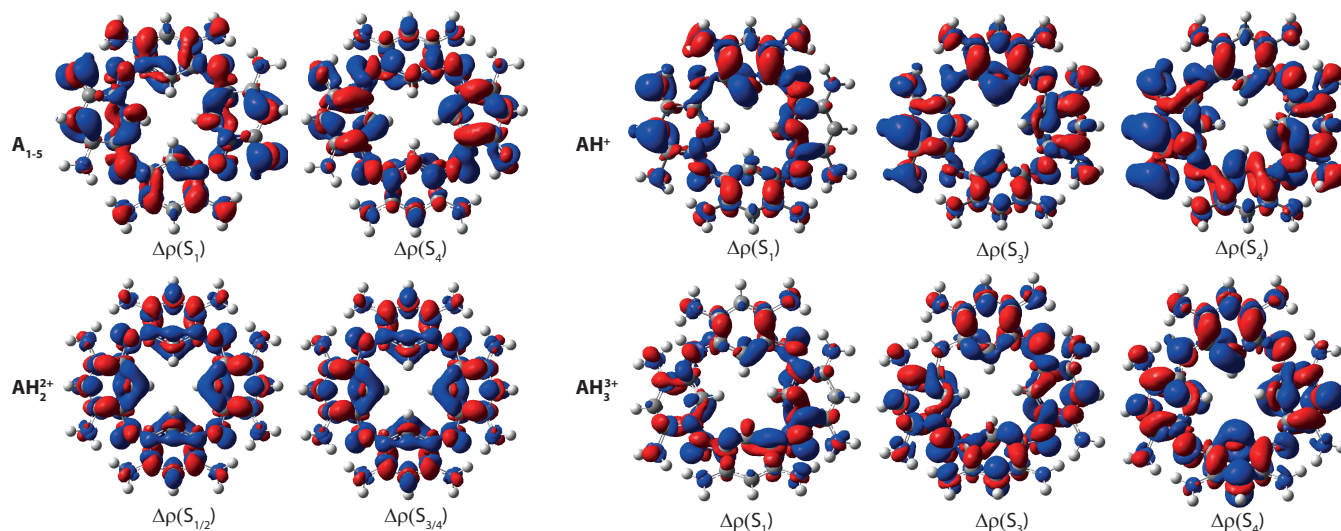


Fig. S6 Electronic density difference (isovalue=0.0008 a.u.) corresponding to the first two absorption bands of the protonated and non-protonated ACP monomers. Red/blue regions indicate gain/loss of electronic density upon photon absorption.

S3 Additional data for the single-bonded derivatives

S3.1 Di-protonated form

Table S3 PBE0 and CAM-B3LYP maximal vertical absorption wavelengths (λ_{abs} in nm) of the first two bands of the di-protonated **Y**-substituted ACP derivatives (Figures 3a and 3b with R=Et). The difference between the two functionals ($\Delta E^{\text{PBE0-CAM}}$) and the differences between the substituted and non-substituted signatures ($\Delta E_{\text{vs.Y=H}}$) are also given in eV. These data have been taken from the convoluted spectra of Figure 5 in the main text.

Y₁	Y₂	$\lambda_{\text{abs}}^{\text{PBE0}}$		$\lambda_{\text{abs}}^{\text{CAM}}$		$\Delta E^{\text{PBE0-CAM}}$		$\Delta E_{\text{vs.Y=H}}^{\text{PBE0}}$		$\Delta E_{\text{vs.Y=H}}^{\text{CAM}}$	
H	H	794	609	822	567	0.05	-0.15				
Br	H	803	623	825	569	0.04	-0.19	-0.02	-0.05	-0.01	-0.01
Br	Br	813	632	832	572	0.03	-0.21	-0.04	-0.07	-0.02	-0.02
NMe ₂	H	798	614	825	577	0.05	-0.13	-0.01	-0.02	-0.01	-0.04
NMe ₂	NMe ₂	803	620	833	584	0.06	-0.12	-0.02	-0.04	-0.02	-0.06
O	H	776	609	728	563	-0.11	-0.17	0.04	0.00	0.13	0.03
O	O	811	588	903	688	0.16	0.31	-0.03	0.07	-0.20	-0.37
NMe	H	783	606	770	561	-0.03	-0.16	0.02	0.01	0.04	0.03
NMe	NMe	783	568	794	552	0.02	-0.06	0.02	0.15	-0.01	0.07

Table S4 Theoretical [PCM-PBE0/6-311+G(2d,p)] vertical absorption energies (λ_{abs} in nm), oscillator strengths (f), and contributions of the molecular orbitals involved in the first four transitions of the **Y**-substituted **AH₂⁺** species of Table S3. H and L stand for HOMO and LUMO, respectively.

Y₁	Y₂	ES n^o	λ_{abs}	f	Molecular orbitals
H	H	1	794	0.13	H→L (64%), H-1→L+1 (35%)
		2	794	0.07	H-1→L (52%), H→L+1 (47%)
		3	613	0.51	H→L+1 (51%), H-1→L (46%)
		4	601	0.31	H-1→L+1 (63%), H→L (34%)
Br	H	1	804	0.08	H→L+1 (50%), H-1→L (49%)
		2	801	0.10	H→L (56%), H-1→L+1 (43%)
		3	627	0.25	H-1→L+1 (54%), H→L (39%)
		4	621	0.53	H-1→L (49%), H→L+1 (48%)
Br	Br	1	815	0.10	H→L (52%), H-1→L+1 (47%)
		2	811	0.07	H-1→L (52%), H→L+1 (47%)
		3	645	0.23	H→L+1 (47%), H-1→L (45%)
		4	628	0.55	H-1→L+1 (51%), H→L (47%)
NMe ₂	H	1	798	0.15	H→L (68%), H-1→L+1 (31%)
		2	796	0.06	H-1→L (53%), H→L+1 (46%)
		3	619	0.49	H→L+1 (49%), H-1→L (43%)
		4	606	0.24	H-1→L+1 (65%), H→L (29%)
NMe ₂	NMe ₂	1	803	0.16	H→L (71%), H-1→L+1 (27%)
		2	800	0.05	H-1→L (55%), H→L+1 (44%)
		3	623	0.49	H→L+1 (51%), H-1→L (41%)
		4	610	0.19	H-1→L+1 (68%), H→L (25%)
NH ₂	NH ₂	1	889	0.03	H→L (88%), H-1→L+1 (11%)
		2	863	0.03	H→L+1 (67%), H-1→L (31%)
		3	734	0.00	H-2→L (95%)
		4	729	0.11	H-1→L+1 (71%), H-3→L (17%)

Table S5 Theoretical [PCM-CAM-B3LYP/6-311+G(2d,p)] vertical absorption energies (λ_{abs} in nm), oscillator strengths (f), and contributions of the molecular orbitals involved in the first four transitions of the **Y**-substituted AH_2^+ species of Table S3. . H and L stand for HOMO and LUMO, respectively.

Y_1	Y_2	ES n°	λ_{abs}	f	Molecular orbitals
H	H	1	828	0.18	H→L (70%), H-1→L+1 (29%)
		2	814	0.11	H→L+1 (55%), H-1→L (44%)
		3	573	0.53	H-1→L (53%), H→L+1 (43%)
		4	557	0.33	H-1→L+1 (67%), H→L (28%)
Br	H	1	828	0.15	H→L (65%), H-1→L+1 (33%)
		2	822	0.14	H→L+1 (59%), H-1→L (40%)
		3	578	0.53	H-1→L (56%), H→L+1 (40%)
		4	575	0.29	H-1→L+1 (62%), H→L (32%)
Br	Br	1	835	0.16	H→L+1 (61%), H-1→L (37%)
		2	830	0.13	H→L (61%), H-1→L+1 (38%)
		3	591	0.26	H-1→L+1 (58%), H→L (35%)
		4	581	0.54	H-1→L (58%), H→L+1 (37%)
NMe ₂	H	1	833	0.19	H→L (73%), H-1→L+1 (26%)
		2	811	0.10	H→L+1 (54%), H-1→L (45%)
		3	574	0.55	H-1→L (52%), H→L+1 (44%)
		4	558	0.28	H-1→L+1 (69%), H→L (25%)
NMe ₂	NMe ₂	1	841	0.21	H→L (75%), H-1→L+1 (23%)
		2	813	0.09	H→L+1 (53%), H-1→L (46%)
		3	576	0.56	H-1→L (50%), H→L+1 (45%)
		4	559	0.23	H-1→L+1 (72%), H→L (22%)

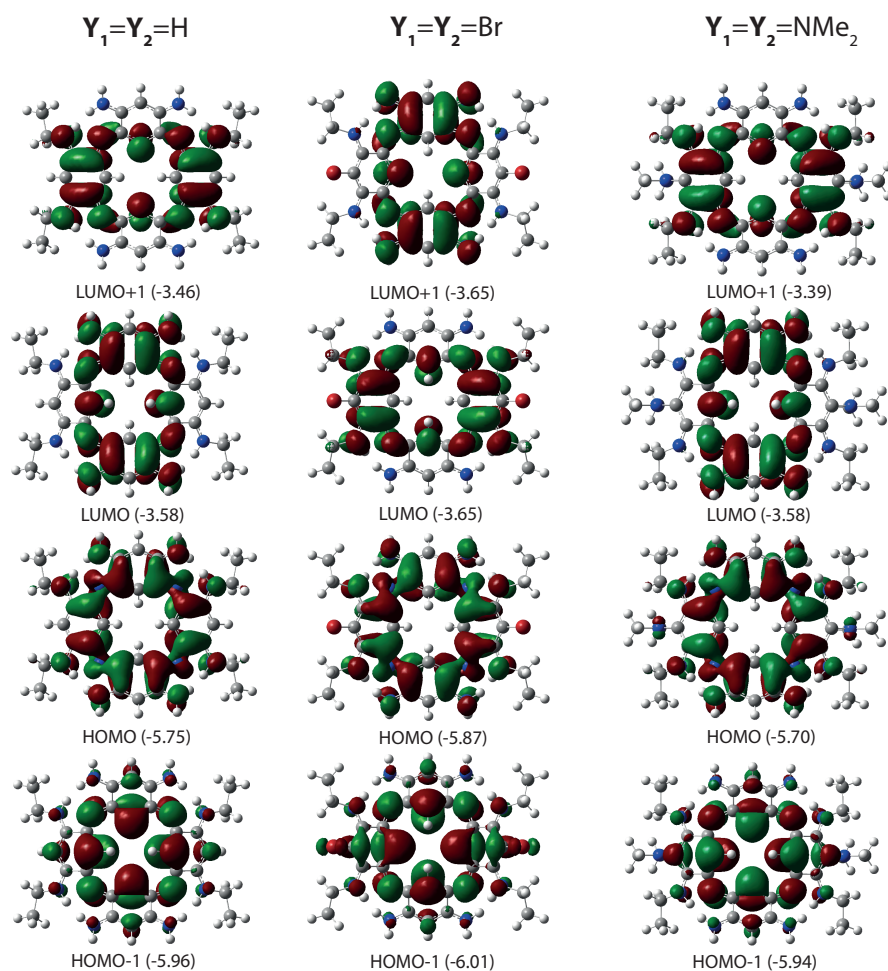


Fig. S7 PBE0 molecular orbitals (isovalue=0.02 a.u.) involved in the first four transitions of symmetrically Y -substituted AH_2^{2+} with $Y_1=Y_2=H$, Br, and NMe_2 and $R=Et$ in Figure 3b. The energies of the orbitals (in eV) are also given in parenthesis. Note the position of the NMe_2 group, almost perfectly perpendicular to the plane of the lateral cyanines.

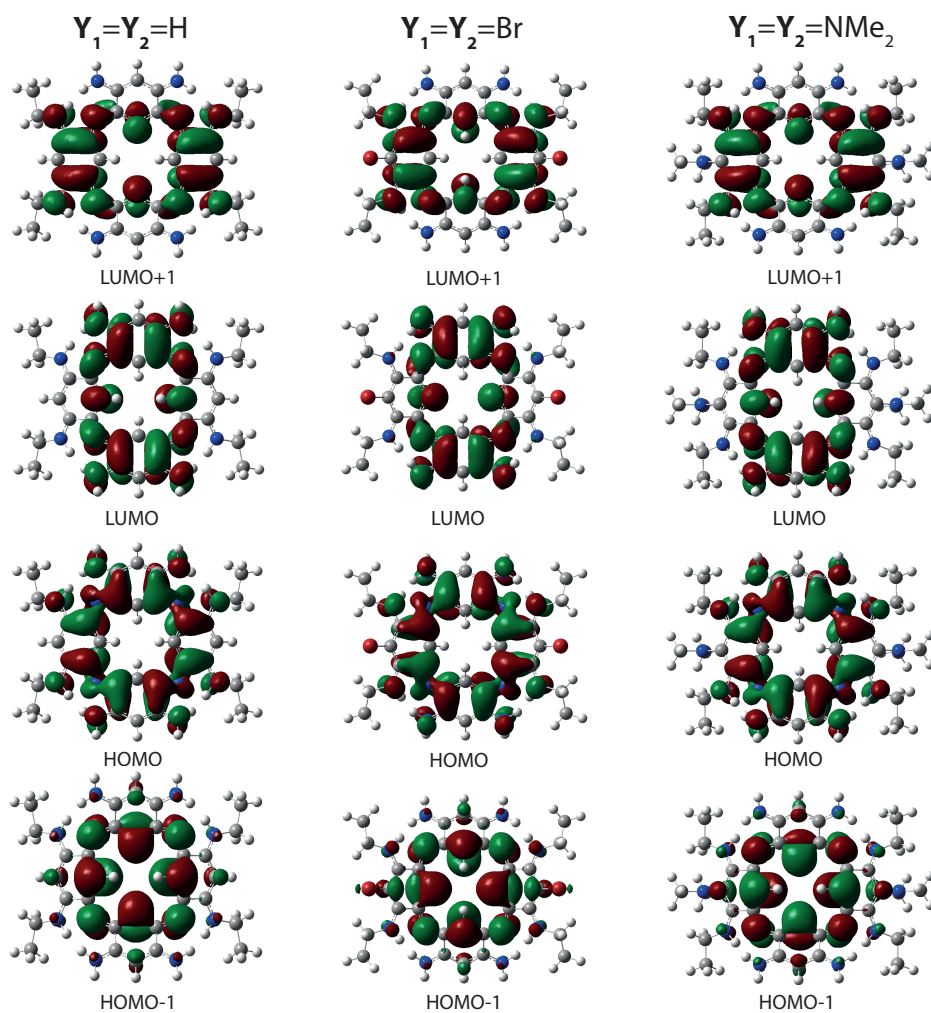


Fig. S8 CAM-B3LYP molecular orbitals (isovalue=0.02 a.u.) involved in the first four transitions of symmetrically Y -substituted AH_2^{2+} . See caption of Figure S7.

S3.2 Other forms

Table S6 Relative PCM-PBE0/6-31G(d) free energies of the tautomeric forms (ΔG_{SBS} in kcal/mol) of **Y**-substituted ACPs in several protonation states displayed in Figure 6 (R=Et). The tautomers give the position of the protonated bridging nitrogen atom (**a** or **b**) for the tri-protonated ACPs or the position of the imino functions (from **1** to **8**) for the mono- and non-protonated ACPs.

State	Y ₁	Y ₂	Tautomer	ΔG_{SBS}	Y ₁	Y ₂	Tautomer	ΔG_{SBS}	Y ₁	Y ₂	Tautomer	ΔG_{SBS}
AH₃³⁺	H	H	—	—	Br	H	a	0.0	NMe ₂	H	a	0.0
					Br	H	b	1.3	NMe ₂	H	b	0.2
					Br	Br	—	—	NMe ₂	NMe ₂	—	—
AH⁺	H	H	1	0.0	Br	H	1	0.0	NMe ₂	H	1	0.0
	H	H	2	4.3	Br	H	2	1.0	NMe ₂	H	2	5.1
					Br	H	5	0.1	NMe ₂	H	5	0.2
					Br	H	6	3.8	NMe ₂	H	6	4.2
					Br	Br	1	0.0	NMe ₂	NMe ₂	1	0.0
					Br	Br	2	1.6	NMe ₂	NMe ₂	2	5.8
A	H	H	1-2	3.1	Br	H	1-2	1.0	NMe ₂	H	1-2	3.9
	H	H	1-3	3.1	Br	H	1-3	0.9	NMe ₂	H	1-3	4.4
	H	H	1-4	0.0	Br	H	1-4	0.9	NMe ₂	H	1-4	0.0
	H	H	1-5	0.7	Br	H	1-5	0.7	NMe ₂	H	1-5	0.8
	H	H	1-6	3.6	Br	H	1-6	3.7	NMe ₂	H	1-6	3.8
	H	H	1-7	2.2	Br	H	1-7	2.6	NMe ₂	H	1-7	1.7
	H	H	1-8	15.2	Br	H	1-8	16.1	NMe ₂	H	1-8	15.0
	H	H	2-3	19.6	Br	H	2-3	15.7	NMe ₂	H	2-3	24.1
	H	H	2-6	8.0	Br	H	2-5	1.8	NMe ₂	H	2-5	5.1
	H	H	2-7	7.3	Br	H	2-6	5.9	NMe ₂	H	2-6	8.6
					Br	H	2-7	5.1	NMe ₂	H	2-7	8.5
					Br	H	2-8	1.1	NMe ₂	H	2-8	3.3
					Br	H	5-6	3.2	NMe ₂	H	5-6	3.0
					Br	H	5-7	3.1	NMe ₂	H	5-7	3.8
					Br	H	5-8	0.0	NMe ₂	H	5-8	1.1
					Br	H	6-7	20.3	NMe ₂	H	6-7	19.7
					Br	Br	1-2	0.5	NMe ₂	NMe ₂	1-2	3.3
					Br	Br	1-3	0.4	NMe ₂	NMe ₂	1-3	4.0
					Br	Br	1-4	0.0	NMe ₂	NMe ₂	1-4	0.0
					Br	Br	1-5	1.3	NMe ₂	NMe ₂	1-5	0.5
					Br	Br	1-6	1.4	NMe ₂	NMe ₂	1-6	4.8
					Br	Br	1-7	0.9	NMe ₂	NMe ₂	1-7	2.5
					Br	Br	1-8	16.3	NMe ₂	NMe ₂	1-8	14.1
					Br	Br	2-3	16.1	NMe ₂	NMe ₂	2-3	23.7
					Br	Br	2-6	4.7	NMe ₂	NMe ₂	2-6	10.2
					Br	Br	2-7	3.9	NMe ₂	NMe ₂	2-7	9.1

Table S7 NICS(0) values (in ppm) at the centre of the macrocycle and of the constitutive rings computed for the most probable tri- and mono-protonated **Y**-substituted ACPs displayed in Figures 6a and 6c, respectively. The tautomers give the position of the protonated bridging nitrogen atom (**a** or **b**) for the tri-protonated ACPs or the position of the imino functions (from **1** to **8**) for the non-protonated ACPs. The value given in bold correspond to six-membered rings bearing one imino function. Their maximal vertical absorption wavelengths (λ_{abs} in nm) and the differences between the substituted and non-substituted (**Y**=H) signatures ($\Delta E_{\text{vs. Y=H}}$ in eV) are also given. The spectroscopic data have been taken from the convoluted spectra (FWHM=1500 cm^{-1}) of Figure 7. All values have been obtained using the PBE0 exchange-correlation functional.

State	Y ₁	Y ₂	Tautomer	O	A	B	C	D	λ_{abs}		$\Delta E_{\text{vs. Y=H}}$	
AH₃³⁺	H	H	—	-8.3	2.4	6.5	5.8	4.1	811	623		
	Br	H	a	-8.1	2.2	6.8	5.5	4.1	809	639	0.00	-0.05
	Br	H	b	-8.6	2.7	3.9	5.8	6.7	819	635	-0.01	-0.04
	Br	Br	—	-8.5	2.4	7.2	5.6	4.1	820	646	-0.02	-0.07
	NMe ₂	H	a	-8.4	2.1	6.5	5.6	3.9	828	626	-0.03	-0.01
	NMe ₂	H	b	-8.3	2.0	3.6	5.5	6.2	810	624	-0.00	-0.00
	NMe ₂	NMe ₂	—	-8.4	1.7	6.3	5.4	3.5	827	627	-0.03	-0.01
AH⁺	H	H	1	-6.4	7.3	5.6	1.9	4.3	805	614		
	Br	H	1	-6.5	7.2	5.2	2.0	4.6	828	630	-0.04	-0.05
	Br	H	2	-6.8	5.5	8.3	2.9	3.8	825	632	-0.04	-0.06
	Br	H	5	-6.3	2.1	3.7	7.0	5.8	841	625	-0.07	-0.04
	Br	Br	1	-6.5	7.0	5.5	2.0	4.0	846	638	-0.07	-0.08
	Br	Br	2	-6.5	5.4	8.1	3.0	3.2	834	645	-0.05	-0.10
	NMe ₂	H	1	-6.2	7.1	5.1	1.6	4.1	799	616	0.01	-0.01
	NMe ₂	H	5	-6.4	1.5	4.0	7.2	5.4	802	616	0.01	-0.01
	NMe ₂	NMe ₂	1	-6.3	7.0	4.9	1.2	3.7	798	619	0.01	-0.02

S4 Additional data for the double-bonded derivatives

S4.1 Di-protonated form

Table S8 Theoretical [PCM-PBE0/6-311+G(2d,p)] absorption energies (λ_{abs} in nm), oscillator strengths (f), and contributions of the molecular orbitals involved in the first four transitions of the di-protonated **Y**-substituted species of Figure 6c and 6d. H and L stand for HOMO and LUMO, respectively.

Y_1	Y_2	ES n°	λ_{abs}	f	Molecular orbitals
H	H	1	794	0.13	H→L (64%), H-1→L+1 (35%)
		2	794	0.07	H-1→L (52%), H→L+1 (47%)
		3	613	0.51	H→L+1 (51%), H-1→L (46%)
		4	601	0.31	H-1→L+1 (63%), H→L (34%)
O	H	1	1652	0.01	H→L (101%)
		2	1233	0.01	H-1→L (97%)
		3	800	0.01	H-1→L+1 (59%), H→L+2 (39%)
		4	775	0.19	H→L+1 (66%), H-1→L+2 (31%)
		5	686	0.00	H-3→L (94%)
		6	672	0.00	H-2→L (98%)
		7	619	0.32	H-1→L+2 (63%), H→L+1 (27%)
		8	603	0.38	H→L+2 (51%), H-1→L+1 (37%)
		9	574	0.07	H-4→L (94%)
O	O	1	1379	0.01	H→L (99%)
		2	1350	0.00	H→L+1 (100%)
		3	1074	0.01	H-1→L (89%), H→L+2 (10%)
		4	1006	0.01	H-1→L+1 (99%)
		5	811	0.36	H→L+2 (74%), H-1→L+3 (14%), H-1→L (11%)
		6	787	0.00	H-1→L+2 (61%), H→L+3 (36%)
		7	701	0.00	H-2→L (99%)
		8	690	0.00	H-2→L+1 (95%)
		9	609	0.01	H-3→L (58%), H-1→L+3 (38%)
		10	595	0.06	H-3→L+1 (80%)
		11	595	0.23	H-1→L+3 (37%), H-3→L (33%), H-3→L+1 (19%)
		12	583	0.00	H-2→L+2 (98%)
		13	583	0.50	H→L+3 (49%), H-1→L+2 (33%), H-3→L+2 (16%)
NMe	H	1	818	0.04	H→L (55%), H-1→L (13%), H→L+1 (15%), H→L+2 (10%)
		2	782	0.06	H→L+2 (30%), H→L (26%), H-1→L (19%), H-1→L+1 (13%), H-1→L+2 (10%)
		3	774	0.07	H→L+1 (63%), H-1→L+2 (23%)
		4	715	0.03	H-1→L+1 (54%), H-1→L (39%)
		5	614	0.43	H-1→L+2 (58%), H→L+1 (19%), H→L (17%)
		6	597	0.41	H→L+2 (49%), H-1→L+1 (26%), H-1→L (18%)
NMe	NMe	1	790	0.16	H-1→L (11%), H→L (53%), H→L+1 (17%)
		2	777	0.13	H→L+1 (41%), H-1→L (18%), H→L (23%)
		3	738	0.00	H→L+1 (23%), H→L+2 (65%)
		4	713	0.00	H→L+3 (45%), H→L+2 (26%), H-1→L (16%), H→L+1 (11%)
		5	665	0.01	H-1→L+1 (85%), H-1→L+3 (10%)
		6	631	0.02	H-1→L+2 (95%)
		7	596	0.33	H-1→L+3 (70%), H→L (19%)
		8	561	0.59	H-1→L (43%), H→L+3 (37%)

Table S9 Theoretical [PCM-CAM-B3LYP/6-311+G(2d,p)] absorption energies (λ_{abs} in nm), oscillator strengths (f), and contributions of the molecular orbitals involved in the first transitions of the di-protonated **Y**-substituted species. H and L stand for HOMO and L, respectively.

Y_1	Y_2	ES n°	λ_{abs}	f	Molecular orbitals
H	H	1	828	0.18	H→L (70%), H-1→L+1 (29%)
		2	814	0.11	H→L+1 (55%), H-1→L (44%)
		3	573	0.53	H-1→L (53%), H→L+1 (43%)
		4	557	0.33	H-1→L+1 (67%), H→L (28%)
O	H	1	1212	0.02	H→L (96%)
		2	791	0.02	H-1→L+1 (54%), H→L+2 (43%)
		3	763	0.13	H→L+1 (59%), H-1→L (23%), H-1→L+2 (15%)
		4	705	0.15	H-1→L (72%), H→L+1 (15%), H-1→L+2 (10%)
		5	572	0.35	H-1→L+2 (66%), H→L+1 (23%)
		6	556	0.43	H→L+2 (50%), H-1→L+1 (39%)
O	O	1	954	0.02	H→L (63%), H→L+1 (31%)
		2	951	0.01	H→L+1 (65%), H→L (30%)
		3	899	0.26	H→L+2 (80%), H-1→L+3 (14%)
		4	784	0.00	H-1→L+2 (52%), H→L+3 (44%)
		5	691	0.01	H-1→L+1 (96%)
		6	687	0.15	H-1→L (91%)
		7	557	0.27	H-1→L+3 (78%), H→L+2 (15%)
		8	529	0.82	H→L+3 (53%), H-1→L+2 (47%)
NMe	H	1	796	0.06	H→L+1 (50%), H-1→L (43%)
		2	764	0.21	H→L (66%), H-1→L+1 (30%)
		3	649	0.02	H→L+2 (92%)
		4	570	0.42	H-1→L+1 (61%), H→L (28%)
		5	552	0.44	H-1→L (47%), H→L+1 (43%)
		6	498	0.03	H-1→L+2 (92%)
		7	459	0.07	H-3→L+1 (36%), H-1→L+3 (34%), H-2→L (17%)
NMe	NMe	1	800	0.28	H→L (74%), H-1→L+1 (22%)
		2	771	0.08	H→L+1 (58%), H-1→L (37%)
		3	598	0.01	H→L+3 (76%), H→L+2 (18%)
		4	557	0.28	H-1→L+1 (63%), H→L (19%), H→L+2 (10%)
		5	550	0.11	H→L+2 (52%), H→L+3 (17%), H→L+1 (10%)

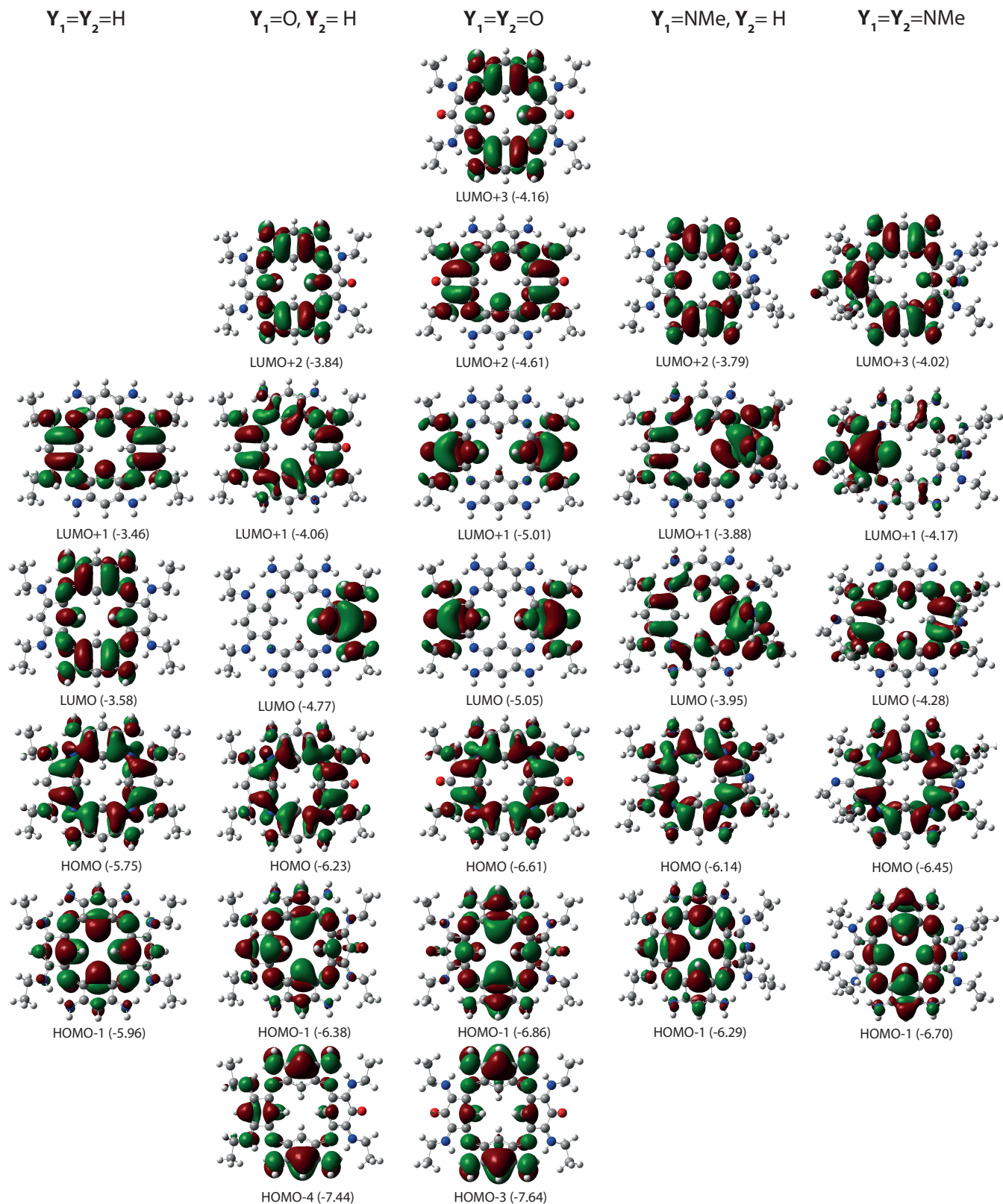


Fig. S9 PBE0 molecular orbitals (isovalue=0.02 a.u.) involved in the first four transitions of symmetrically Y -substituted AH_2^{2+} with $Y=O$ and $Y=NMe$. The energies of the orbitals (in eV) are also given in parenthesis.

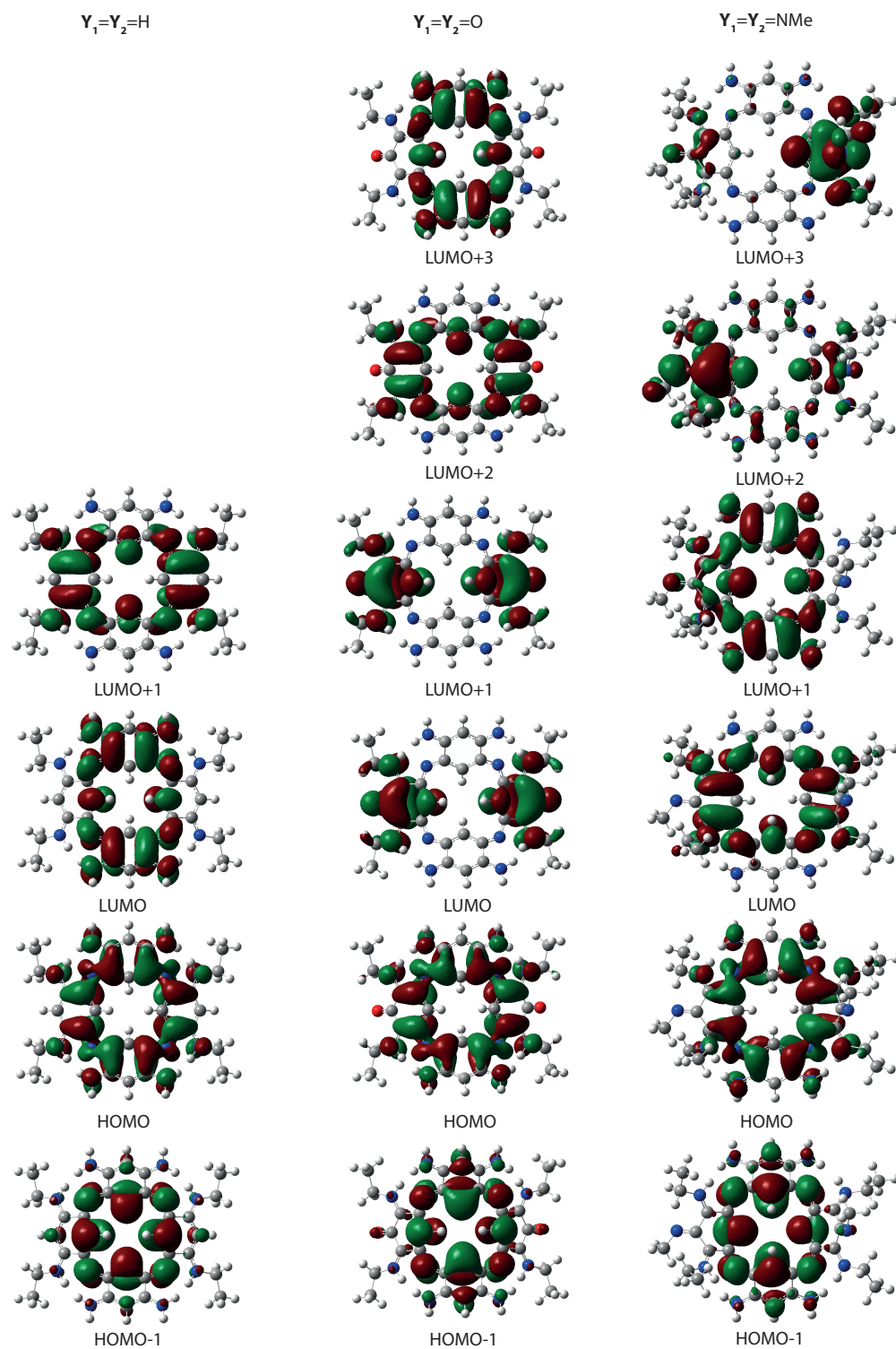


Fig. S10 CAM-B3LYP molecular orbitals (isovalue=0.02 a.u.) involved in the first four transitions of symmetrically di-protonated Y -substituted species with $Y_1=Y_2=H, O,$ and NMe .

Table S10 Gas-phase vertical transition energies (ΔE_{abs} in eV) and oscillator strengths (f) of the first dipole-allowed transitions for **Y**-substituted AH_2^+ species with **Y**=H, O, and NMe, using the *aug-cc-pVDZ* atomic basis set. The difference between the two functionals with CC2 ($\Delta E_{\text{vs. CC2}}$) are also given in eV. CAM stands for CAM-B3LYP.

Y ₁	Y ₂	$\Delta E_{\text{abs}}^{\text{CC2}} (f)$	$\Delta E_{\text{abs}}^{\text{PBE0}} (f)$	$\Delta E_{\text{abs}}^{\text{CAM}} (f)$	$\Delta E_{\text{vs. CC2}}^{\text{PBE0}}$	$\Delta E_{\text{vs. CC2}}^{\text{CAM}}$
H	H	1.624 (0.12)	1.580 (0.09)	1.524 (0.12)	0.04	0.10
		2.106 (0.44)	2.099 (0.40)	2.244 (0.42)	0.01	0.14
O	H	1.570 (0.14)	1.645 (0.10)	1.784 (0.15)	0.08	0.21
		2.023 (0.27)	2.088 (0.21)	2.226 (0.26)	0.07	0.20
O	O	1.598 (0.33)	1.558 (0.23)	1.428 (0.23)	0.04	0.17
		2.163 (0.09)	2.068 (0.13)	2.298 (0.14)	0.09	0.14
NMe	H	1.592 (0.07)	1.646 (0.05)	1.706 (0.13)	0.05	0.11
		2.072 (0.33)	2.046 (0.11)	2.225 (0.28)	0.03	0.15
		2.096 (0.39)	2.061 (0.30)	2.291 (0.21)	0.04	0.19
NMe	NMe	1.569 (0.21)	1.579 (0.09)	1.567 (0.23)	0.10	0.00

S4.2 Other forms

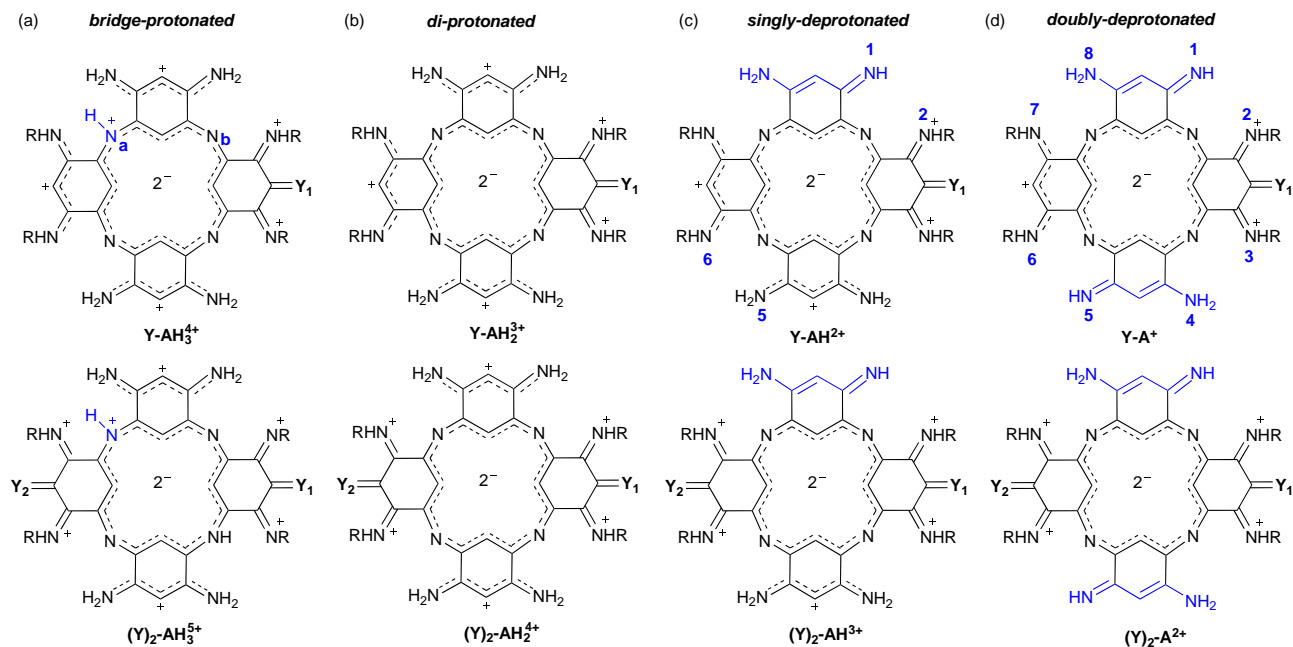


Fig. S11 Representation of the asymmetrically (top) and symmetrically (bottom) structures of the (a) bridge-protonated, (b) di-protonated, (c) singly-deprotonated, and (d) doubly-deprotonated Y-substituted ACPs. The changes upon protonation/deprotonation of the di-protonated ACP are highlighted in blue. The position of the protonated bridging nitrogen atom (**a** or **b**) and of the imino groups (from **1** to **8**) are labeled on the structures at the top.

Table S11 Relative free energies (ΔG in kcal/mol) computed at the PCM-PBE0/6-31G(d) level of theory for Y-substituted (with Y=O and Y=NMe) ACPs in several protonation states. The label of the tautomers are displayed in Figure S11.

State	Y ₁	Y ₂	Tautomer	ΔG	Y ₁	Y ₂	Tautomer	ΔG
Bridge-protonated	O	H	a	0.0	NMe	H	a	0.0
	O	H	b	2.8	NMe	H	b	4.4
	O	O	—	—	NMe	NMe	—	—
Singly-deprotonated	O	H	1	17.2	NMe	H	1	17.3
	O	H	2	0.0	NMe	H	2	0.0
	O	H	5	17.6	NMe	H	5	17.2
	O	H	6	20.1	NMe	H	6	20.6
	O	O	1	19.5	NMe	NMe	1	19.8
	O	O	2	0.0	NMe	NMe	2	0.0
Doubly-deprotonated	O	H	1-2	14.4	NMe	H	1-2	15.3
	O	H	1-3	12.6	NMe	H	1-3	11.1
	O	H	1-4	30.6	NMe	H	1-4	29.8
	O	H	1-5	28.9	NMe	H	1-5	29.1
	O	H	1-6	32.3	NMe	H	1-6	32.3
	O	H	1-7	31.9	NMe	H	1-7	32.3
	O	H	1-8	43.3	NMe	H	1-8	46.3
	O	H	2-3	0.0	NMe	H	2-3	0.0
	O	H	2-5	12.4	NMe	H	2-5	15.3
	O	H	2-6	15.6	NMe	H	2-6	19.1
	O	H	2-7	16.3	NMe	H	2-7	19.5
	O	H	2-8	12.9	NMe	H	2-8	14.7
	O	H	5-6	32.6	NMe	H	5-6	32.4
	O	H	5-7	31.8	NMe	H	5-7	31.3
	O	H	5-8	28.5	NMe	H	5-8	27.7
	O	H	6-7	48.7	NMe	H	6-7	49.8
	O	O	1-2	17.8	NMe	NMe	1-2	17.3
	O	O	1-3	17.5	NMe	NMe	1-3	20.5
	O	O	1-4	36.4	NMe	NMe	1-4	37.4
	O	O	1-5	37.6	NMe	NMe	1-5	37.8
	O	O	1-6	17.6	NMe	NMe	1-6	18.6
O	O	1-7	18.4	NMe	NMe	1-7	23.4	
O	O	1-8	49.1	NMe	NMe	1-8	53.2	
O	O	2-3	3.5	NMe	NMe	2-3	5.0	
O	O	2-6	0.0	NMe	NMe	2-6	0.0	
O	O	2-7	0.0	NMe	NMe	2-7	3.4	

Table S12 PCM-PBE0/6-311+G(2d,p) vertical absorption energies (λ_{abs} in nm), oscillator strengths (f), and contributions of the molecular orbitals involved in the first four dipole-allowed ($f > 0.5$) transitions for the bridge-protonated **Y**-substituted species with **Y**=H, O, and NMe. The transitions for the asymmetrically substituted ACPs are reported for the most stable **a** tautomer. H and L stand for HOMO and LUMO, respectively.

Y ₁	Y ₂	ES n ^o	λ_{abs}	f	Molecular orbitals
H	H	1	813	0.27	H→L (81%), H-1→L+1 (15%)
		3	626	0.42	H→L+1 (54%), H-1→L (39%)
		4	598	0.11	H-1→L+1 (78%), H→L (14%)
		7	516	0.08	H-4→L (71%), H-2→L+1 (12%)
O	H	3	762	0.22	H→L+1 (59%), H→L+2 (14%), H-1→L+2 (13%)
		4	739	0.12	H→L+2 (38%), H-1→L+1 (34%), H→L+1 (15%)
		6	619	0.25	H-1→L+1 (37%), H→L+2 (27%), H-1→L+2 (15%), H-2→L (10%)
		8	589	0.13	H-1→L+2 (49%), H-1→L+1 (11%), H-3→L (10%)
O	O	3	892	0.09	H-1→L (47%), H→L+2 (43%)
		5	816	0.26	H-1→L (40%), H→L+2 (36%)
		10	618	0.18	H→L+3 (33%), H-1→L+3 (22%), H-2→L+2 (12%)
		11	583	0.12	H-1→L+3 (67%)
NMe	H	1	773	0.24	H→L (81%), H-1→L+1 (15%)
		2	758	0.08	H→L+1 (53%), H-1→L (42%)
		4	619	0.31	H-1→L (46%), H→L+1 (35%), H-1→L+1 (11%)
		5	587	0.15	H-1→L+1 (63%), H→L (10%)
NMe	NMe	1	813	0.32	H→L (86%)
		4	644	0.10	H→L+3 (33%), H→L+1 (23%), H→L+2 (20%), H-1→L (13%)
		6	606	0.16	H-1→L+1 (37%), H→L+1 (18%), H→L+3 (18%)
		7	577	0.18	H-1→L+1 (46%), H-2→L (13%)

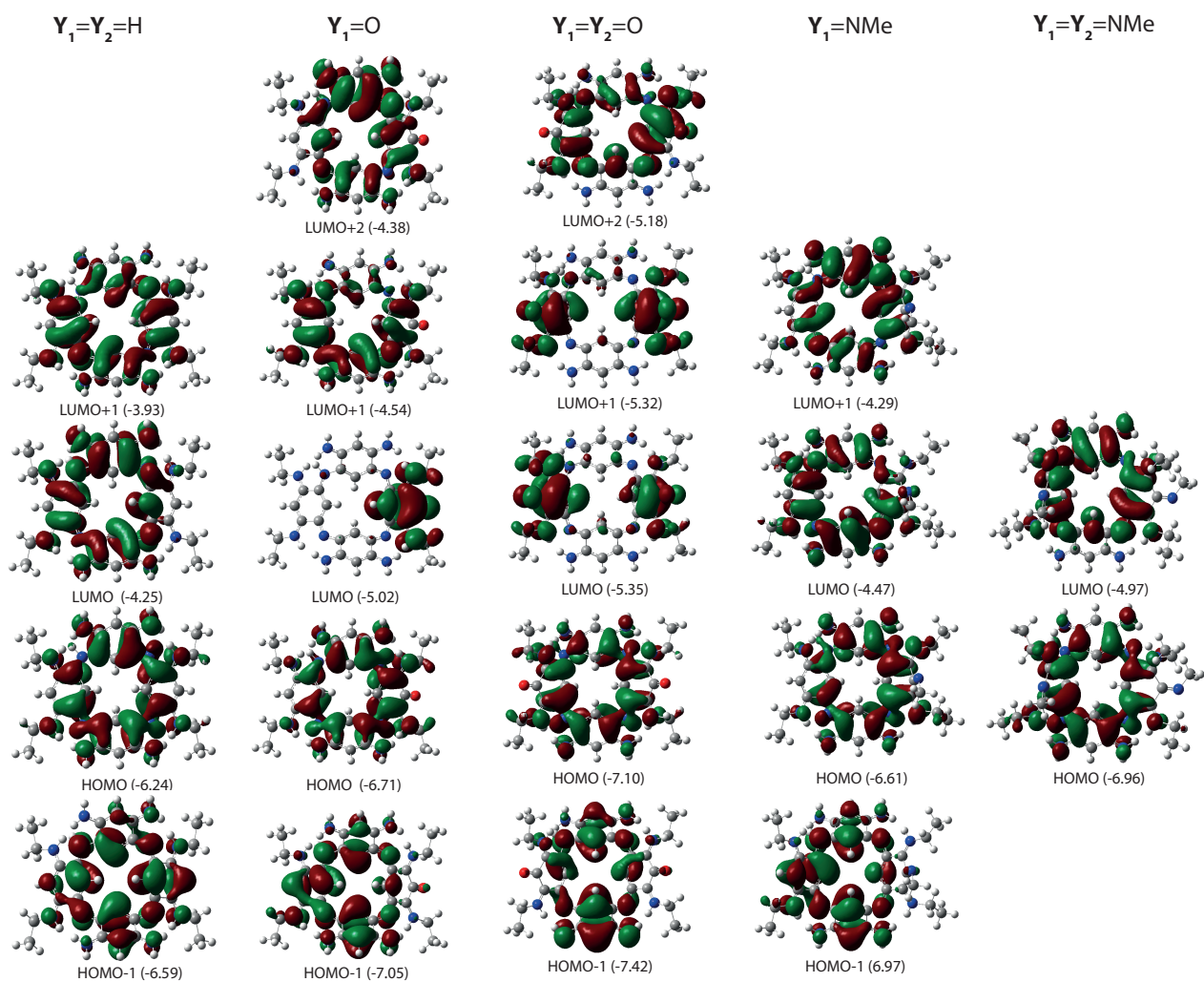


Fig. S12 PBE0 molecular orbitals (isovalue=0.02 a.u.) involved in the lowest transitions of bridge-protonated Y -substituted ACPs with $Y=H$, O , and NMe . For asymmetric derivatives, the most stable **a** tautomer. The energies of the orbitals (in eV) are also given in parenthesis.

Table S13 Theoretical [PCM-PBE0/6-311+G(2d,p)] vertical absorption energies (λ_{abs} in nm), oscillator strengths (f), and contributions of the molecular orbitals involved in the first four dipole-allowed ($f > 0.5$) transitions for the singly-deprotonated Y-substituted species with Y=H, O, and NMe. Only the transitions for the most stable ACPs are reported, that is, tautomer 1 for Y=H and tautomer 2 for Y=O and Y=NMe derivatives. H and L stand for HOMO and LUMO, respectively.

Y ₁	Y ₂	ES n°	λ_{abs}	f	Molecular orbitals
H	H	1	815	0.18	H→L (77%), H-1→L+1 (21%)
		2	768	0.07	H→L+1 (52%), H-1→L (46%)
		3	618	0.32	H-1→L+1 (35%), H-1→L (28%), H→L+1 (21%), H→L (12%)
		4	609	0.32	H-1→L+1 (39%), H→L+1 (25%), H-1→L (23%)
O	H	1	998	0.08	H→L (75%), H-1→L+1 (20%)
		2	869	0.08	H-1→L+2 (58%), H→L+1 (20%), H→L (19%)
		4	716	0.28	H→L+1 (60%), H-1→L (16%), H-1→L+2 (16%)
		5	599	0.37	H→L+2 (47%), H-1→L+1 (43%)
O	O	3	930	0.12	H→L+1 (78%)
		5	695	0.16	H→L+2 (50%), H→L+3 (21%), H-1→L+3 (14%)
		7	677	0.17	H→L+3 (33%), H-1→L+2 (30%), H-1→L+1 (18%)
		8	600	0.11	H-1→L+3 (33%), H-1→L+1 (22%), H-1→L+2 (22%)
NMe	H	1	811	0.11	H→L+1 (59%), H-1→L (34%)
		2	791	0.15	H→L+1 (66%), H-1→L+1 (27%)
		3	646	0.18	H-1→L (34%), H-1→L+1 (21%), H→L+1 (17%), H→L+2 (16%), H→L (10%)
		4	609	0.38	H-1→L+1 (40%), H-1→L (24%), H→L+1 (17%), H→L (12%)
NMe	NMe	2	780	0.12	H→L (36%), H-1→L+2 (19%), H→L+1 (19%), H→L+2 (14%)
		3	755	0.06	H→L+2 (37%), H→L+1 (25%), H-1→L (25%)
		5	612	0.29	H-1→L+2 (67%), H→L (14%)
		6	583	0.48	H→L+2 (36%), H-1→L (30%), H-1→L+1 (14%)

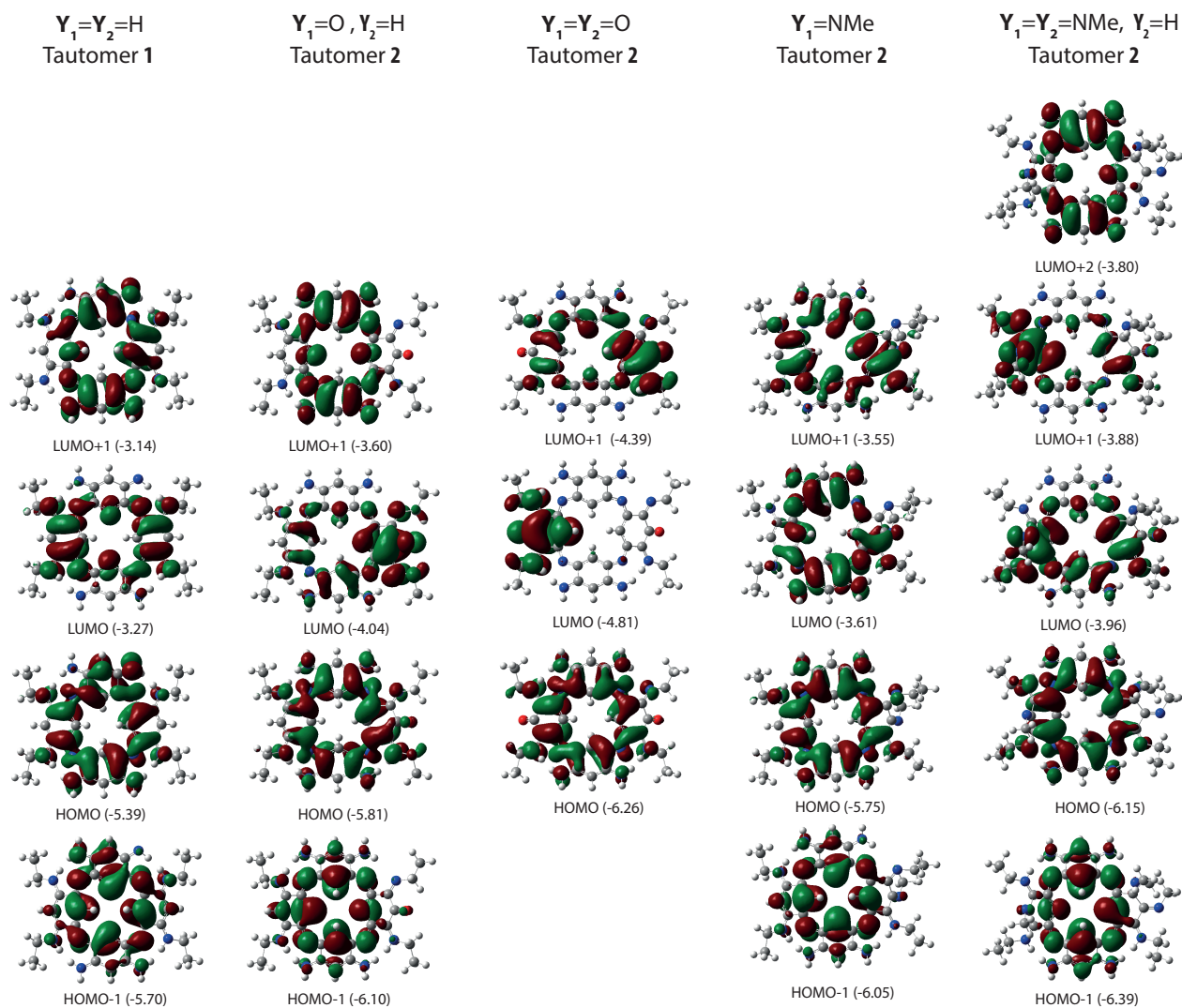


Fig. S13 PBE0 molecular orbitals (isovalue=0.02 a.u.) involved in the first transitions of singly-deprotonated Y -substituted ACPs with $Y=H, O,$ and NMe . The energies of the orbitals (in eV) are also given in parenthesis.

Table S14 Theoretical [PCM-PBE0/6-311+G(2d,p)] absorption energies (λ_{abs} in nm), oscillator strengths (f), and contributions of the molecular orbitals involved in the first four dipole-allowed ($f > 0.5$) transitions for the doubly-deprotonated **Y**-substituted species with **Y**=O or **Y**=NMe₂. H and L stand for HOMO and LUMO, respectively.

Y₁	Y₂	Tautomer	ES n^o	λ_{abs}	f	Molecular orbitals
O	H	2-3	1	799	0.22	H→L+1 (82%), H-1→L+1 (17%)
			4	603	0.51	H-1→L+1 (60%), H-1→L (36%)
			5	566	0.25	H-1→L+1 (79%), H→L (16%)
			10	449	0.09	H→L+3 (92%)
O	O	2-6	1	1095	0.11	H→L (81%), H-1→L (16%)
			3	887	0.12	H-1→L (64%), H-1→L+2 (20%), H-1→L (15%)
			5	699	0.0.40	H→L+2 (69%), H-1→L (19%), H-1→L+3 (10%)
			8	580	0.24	H→L+3 (47%), H-1→L+2 (37%)
O	O	2-7	1	1062	0.14	H→L (94%)
			4	749	0.15	H-1→L+1 (85%)
			5	697	0.30	H→L+2 (68%), H-1→L (21%), H-1→L+3 (10%)
			7	584	0.24	H-1→L+2 (44%), H→L+3 (43%)
NMe	H	2-3	1	799	0.23	H→L (83%), H-1→L+1 (16%)
			3	602	0.53	H→L+1 (62%), H-1→L (34%)
			4	565	0.24	H-1→L+1 (81%), H→L (15%)
			10	423	0.19	H-2→L+1 (85%)
NMe	NMe	2-6	1	829	0.16	H→L (76%), H-1→L+1 (23%)
			2	780	0.15	H→L+1 (73%), H-1→L (26%)
			4	637	0.24	H-1→L+1 (51%), H-1→L (19%), H→L (13%)
			5	598	0.41	H-1→L (48%), H-1→L+1 (17%), H→L+1 (14%)

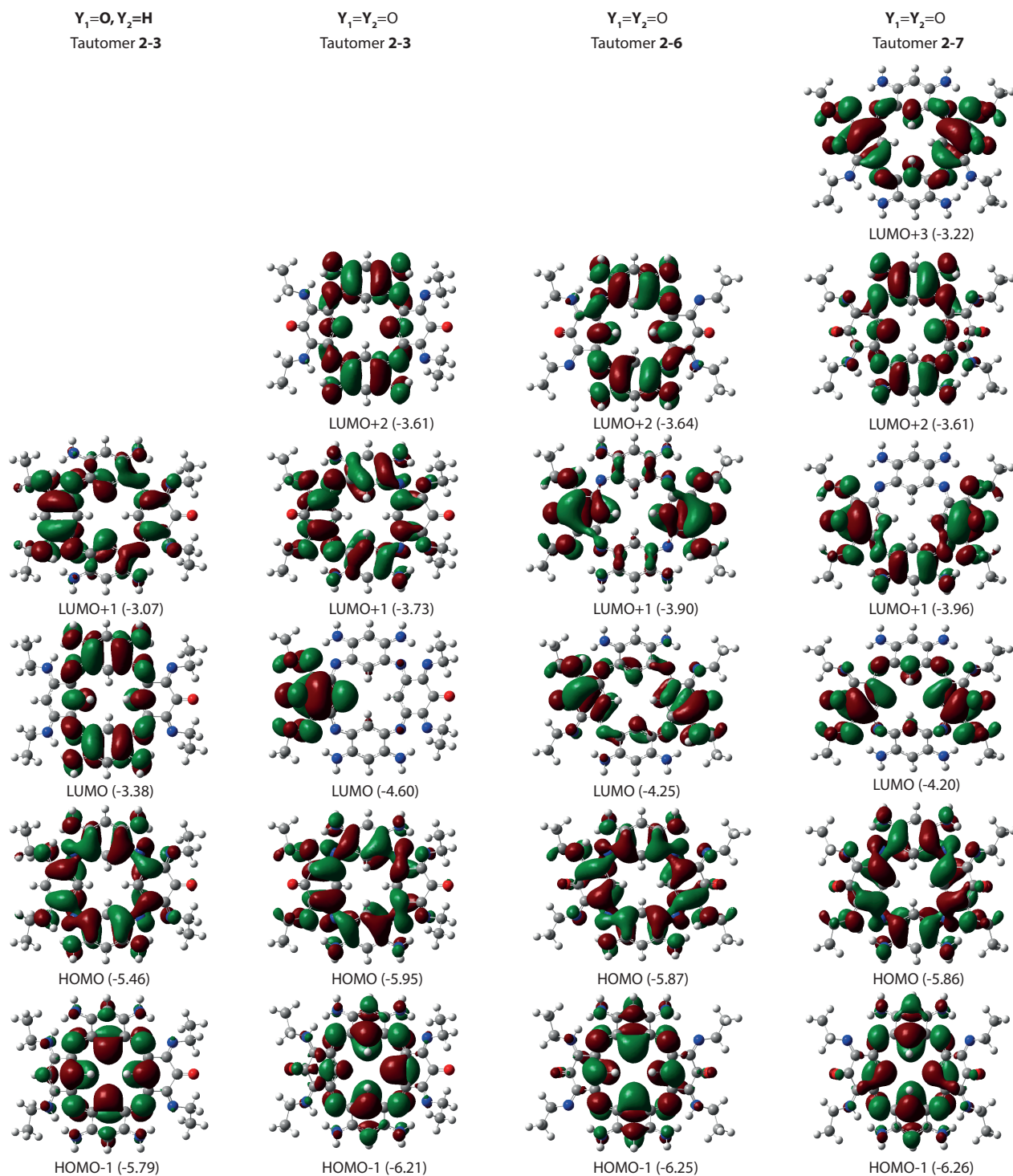


Fig. S14 PBE0 molecular orbitals (isovalue=0.02 a.u.) involved in the first transitions of doubly-deprotonated keto-derivatives. The energies of the orbitals (in eV) are also given in parenthesis.

References

- 1 Z. Chen, M. Giorgi, D. Jacquemin, M. Elhabiri and O. Siri, *Angew. Chem. Int. Ed.*, 2013, **52**, 6250–6254.
- 2 G. Marchand, P. Giraudeau, Z. Chen, M. Elhabiri, O. Siri and D. Jacquemin, *Phys. Chem. Chem. Phys.*, 2016, **18**, 9608–9615.
- 3 P. C. Chen and Y. C. Chieh, *J. Mol. Struct. (THEOCHEM)*, 2003, **624**, 191–200.
- 4 A. D. Laurent and D. Jacquemin, *Int. J. Quantum Chem.*, 2013, **113**, 2019–2039.